Heterogeneous & Homogeneous & Bio- & Nano-
CHEMCATCHEM
CATALYSIS

Accepted Article

Title: Comparative Study of Diverse Cu-Zeolites for Conversion of Methane-to-Methanol

Authors: Min Bum Park, Sang Hyun Ahn, Marco Ranocchiari, and Jeroen van Bokhoven

To be cited as: *ChemCatChem* 10.1002/cctc.201700768

Link to VoR: http://dx.doi.org/10.1002/cctc.201700768

A Journal of
ChemPubSoc Europe

WILEY-VCH

www.chemcatchem.org

Comparative Study of Diverse Cu-Zeolites for Conversion of Methane-to-Methanol

Min Bum Park,[a, b] Sang Hyun Ahn,[c] Marco Ranocchiari,[b] and Jeroen A. van Bokhoven*[a, b]

Abstract: The characterization and reactive properties of Cu-zeolites with twelve framework topologies (MOR, EON, MAZ, MEI, BPH, FAU, LTL, MFI, HEU, FER, SZR, and CHA) are compared in the stepwise partial oxidation of methane-to-methanol. Cu^{2+} ion-exchanged zeolite omega, a MAZ-type material, reveals the highest yield (86 μmol g-cat.$^{-1}$) among these materials after high-temperature activation and liquid methanol extraction. The high yield is ascribed to the relatively high density of copper-oxo active species, which form in its three-dimensional 8-membered (MB) ring channels. In-situ UV-Vis shows that diverse copper species form in different zeolites after high-temperature activation, suggesting that there are no universally active species. Nonetheless, there are some dominant factors required for achieving high methanol yields: i) highly dispersed copper-oxo species; ii) large amount of exchanged copper in small-pore zeolites; iii) moderately high temperature of activation; iv) use of proton form zeolite precursors. Cu-omega and Cu-mordenite, with the proton form of mordenite as the precursor, yield methanol after activation in oxygen and reaction with methane at only 200 °C, i.e., under isothermal conditions.

Introduction

One of the reasons why methane is still an underutilized feedstock is because its transport from remote drill sites is difficult. Furthermore, because of the increasing availability of cheap natural gas, the conversion of methane into more easily transportable liquids or into chemicals is a very desirable goal.[1] Although the visible applicability for direct methane upgrading is still a long way off, the low temperature partial oxidation of methane-to-methanol over metal-containing zeolites mimics enzymatic systems.[2] The pentasil zeolites, such as ZSM-5 (framework type MFI) and mordenite (MOR), which are representative commercial medium- and large-pore zeolites, respectively, stabilize binuclear[3] and trinuclear[4] oxide compounds of iron and/or copper, which are structurally analogous to those found in methane monooxygenases. Over the past decade, several research groups have focused on these reaction systems to evaluate the nature of active core species by means of diverse spectroscopic characterization tools as well as computational analyses.[3-20] Recently, Grundner et al. reported that single-site trinuclear copper-oxo species can be stabilized in mordenite and that Cu-mordenite showed the highest total yield of methane oxidation products.[4a] In general, when comparing iron- and copper-containing zeolite systems, even though the Cu-zeolites have some advantages, i.e., lower activation temperature, possible use of either nitrous oxide or oxygen as an oxidant, etc., the major disadvantage of this system is the considerably lower methanol yield than that of iron-based systems.[1b,9]

There are many hurdles to overcome before these transition metal zeolites can be implemented for the conversion of methane-to-methanol. The intermediate, chemisorbed methoxy species, does not readily desorb from the active sites formed in zeolite pores under the continuous reaction conditions, and there is no methanol at the reactor outlet. When the temperature is above 200 °C in order to desorb the methanol it undergoes deeper oxidation to CO and/or CO_2.[12] Therefore, it is necessary to extract the methanol in an additional step.[6,12] Exposing oxygen-activated and methane-reacted Cu-zeolites to steam releases methanol, enabling cyclic operation.[3a,16]

As well as the two best known zeolites, mordenite and ZSM-5, other commercial zeolites are also known.[6,7,18] Cu^{2+} ion-exchanged ferrierite (FER) and beta (*BEA) zeolites, medium- and large-pore zeolites, respectively, resulted in comparable amounts of extracted methanol as Cu-ZSM-5. Recently, some small-pore copper-containing zeolite materials (SSZ-13 (CHA), SSZ-16 (AFX), and SSZ-39 (AEI)) showed a good methane-to-methanol performance.[16-18] The amount of produced methanol from these small-pore zeolites is greater than those with mordenite and ZSM-5 under identical conditions. However, there are still relatively few published data on the other structure types of zeolites in this reaction.

There are two large-pore zeolites with a structure similar to that of mordenite, i.e., EON- and MAZ-type zeolites.[21,22] The EON structure is composed of strictly alternating *maz* and *mor* layers, from which the well-known MAZ and MOR structures are built, connected by five-ring chains in a regular 1:1 stacking sequence. The EON structure has one-dimensional (1D) 12-membered (MB) ring channels interconnected by 8-MB ring channels like those of MOR but the channel system is much more complicated than those of MOR and MAZ (Table 1). The MAZ structure is also composed of 1D and 3D 12- and 8-MB ring channels, respectively. However, unlike MOR and EON, the

[a] Prof. Dr. M. B. Park,[+] Prof. Dr. J. A. van Bokhoven
Institute for Chemical and Bioengineering
ETH Zürich
Zürich 8093 (Switzerland)
E-mail: jeroen.vanbokhoven@chem.ethz.ch
[b] Prof. Dr. M. B. Park,[+] Dr. M. Ranocchiari, Prof. Dr. J. A. van Bokhoven
Laboratory for Catalysis and Sustainable Chemistry
Paul Scherrer Institute
Villigen 5232 (Switzerland)
[c] S. H. Ahn
School of Environmental Science and Engineering
POSTECH
Pohang 37673 (Korea)
[+] Present address: Department of Energy and Chemical Engineering, Incheon National University, Incheon 22012 (Korea)

Supporting information for this article is given via a link at the end of the document.

two-channel systems are not interconnected. MEI and BPH also contain 1D 12-MB ring channels interconnected by small-pore channels.[21,23] Both structures have the same secondary building unit, *mei*, but its connecting mode differs slightly. As a result, both structures have three side-pockets around the channel, perpendicular to the *c*-axis, but only those of MEI are rotated to 60° along the *c*-axis. PST-11, a new MEI-type zeolite, was synthesized using the two simplest organic structure-directing agents (SDAs), i.e., tetramethylammonium (TMA^+) and tetraethylammonium (TEA^+) ions, based on the charge density mismatch synthesis method.[24] PST-11 has a much higher aluminum content (Si/Al = 3.4 vs 4.8) than UZM-22, which is another MEI-type zeolite.[23]

We report the catalytic properties of copper-containing large-pore zeolites with five different framework topologies (Table 1) for the methane-to-methanol conversion reaction by varying the Si/Al ratios, copper contents, and ion-exchanged precursor types as well as the activation temperatures in a flow of oxygen. We also tested seven well-known large-, medium-, and small-pore zeolites (Y (FAU), L (LTL), ZSM-5, clinoptilolite (HEU), ferrierite, SUZ-4 (SZR), and SSZ-13) listed in the Supporting Information Table S1 for comparison. Based on the results, we suggest some guidelines for developing more active materials for this reaction based on structural and chemical features.

Table 1. Structural features, chemical composition, and nitrogen sorption data for the large-pore zeolites in this study.

Material	IZA code	Structural features (pore size, a x b)[a] (Å)		Si/Al	BET surface area[b] ($m^2\ g^{-1}$)
Mordenite	MOR	[001] 12 (6.5 x 7.0)* ↔ [001] 8 (2.6 x 5.7)***	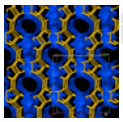	8.5 5.0	460 400
ECR-1	EON	{[100] 12 (6.6 x 7.4)* ↔ [010] 8 {[001] (3.4 x 4.9) ↔ [100] 8 (2.9 x 2.9)}*}**	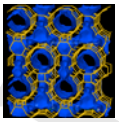	3.5	520
Omega	MAZ	[001] 12 (7.4 x 7.4)* | [001] 8 (3.1 x 3.1)***	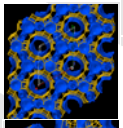	3.2	360
PST-11 UZM-22	MEI	[001] 12 (6.9 x 6.9)* ↔ ⊥ [001] 7 (3.2 x 3.5)**	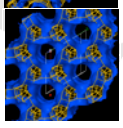	3.4 4.8	660 630
UZM-4	BPH	[001] 12 (6.3 x 6.3)* ↔ ⊥ [001] 8 (2.7 x 3.5)**	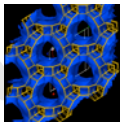	3.0	540

[a] Referenced according to the Database of Zeolite Structures.[21] [b] Determined by using the calcined or proton form.

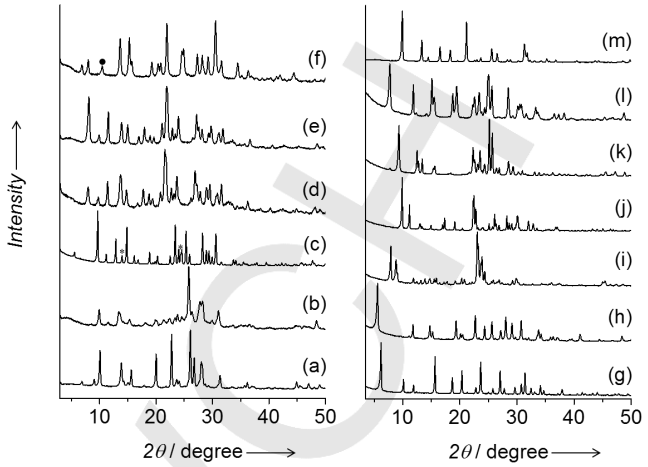

Figure 1. Powder XRD patterns of (a) CuNa-mordeniteH, (b) CuNa-ECR-1H, (c) CuNa-omegaH, (d) CuNa-PST-11H, (e) CuNa-UZM-22H, (f) CuNa-UZM-4H, (g) CuNa-YH, (h) CuNa-LH, (i) CuNa-ZSM-5H, (j) CuNa-clinoptiloliteH, (k) CuNa-ferrieriteH, (l) CuNa-SUZ-4H, and (m) CuNa-SSZ-13H. The X-ray peaks from sodalite and unidentified copper derivative are marked by asterisk and filled circle, respectively.

Results and Discussion

Catalyst characterization

Figure 1 shows the powder XRD patterns of Cu^{2+} ion-exchanged zeolites. When compared to those of parent zeolites in the Supporting Information Figure S1, the lack of reflections of copper and its oxides in all the patterns, with the exception of CuNa-UZM-4H, indicates the absence of large copper-containing particles. The reflection around 2θ = 10.5° in the pattern of CuNa-UZM-4H does not originate from the BPH structure. The intensity of this peak increased with copper content (see Figure S2). This implies the presence of an unknown copper-containing species. All the materials were structurally stable after activation at 450 or 550 °C and reaction with methane (see Figure S3).

Figure 2 shows the TEM images of representative copper-containing samples, i.e., mordenite, omega, and PST-11 with 3.1, 5.9, and 8.4 wt. % of copper, respectively (Table 2). The TEM images showed intact zeolite channels and well dispersed copper particles (dark gray dots) with a mean particle size of around 1.8, 2.1, and 2.6 nm in each fresh Cu-zeolite; some of the particles sinter under prolonged exposure to the electron beam.[10] The TEM images of CuNa-omegaH and CuNa-PST-11H, with a relatively large amount of copper, revealed clearer images of highly dispersed copper particles even after activation at 550 °C although the size became a little larger than the fresh one. The copper species should be changed to copper oxides during the activation in a flow of oxgen. However, those were still not detected in the powder XRD patterns (see Figure S3).

Table 2 lists the chemical composition and nitrogen sorption data for the various Cu^{2+} ion-exchanged zeolite materials prepared in this study. As expected, the resulting ion-exchanged

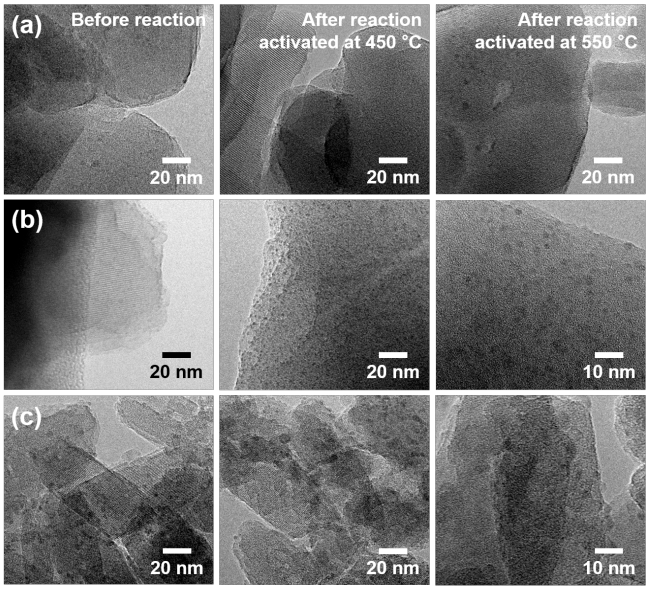

Figure 2. TEM images of (a) CuH-mordeniteH, (b) CuNa-omegaH, and (c) CuNa-PST-11H before reaction (left) and after reaction activated at 450 °C (middle) and 550 °C (right).

copper content (wt. %) is generally higher in the zeolites with a lower Si/Al ratio. For example, when comparing CuNa-PST-11H (Si/Al = 3.4) with CuNa-UZM-22H (Si/Al = 4.8), both of which have the same zeolite framework topology (MEI), the copper content is almost twice as high in the CuNa-PST-11H (8.4 vs 4.3 wt. %). On the other hand, despite the same Si/Al ratio (5.0) and an identical ion-exchange procedure, the resulting copper content (3.1 vs 4.4 wt. %) of CuH-mordeniteH is lower than that of CuNa-mordeniteH. The situation was similar for ECR-1, omega, and UZM-22. The differences in the copper contents are large for ECR-1 and omega and small for UZM-22. It has been reported that the Cu^{2+}-exchange level of Na-ZSM-5 decreased with decreasing pH of the solution. The presence of H^+ cations in the solution inhibits the ion exchange between Cu^{2+} and Na^+ cations.[25] Compared to CuNa-ECR-1H, the pH of the CuH-ECR-1H solution right after ion-exchange in one cycle, the latter one (5.9 vs 5.5) decreased to a greater extent from the initial pH (6.0) of 0.01 M Cu^{2+} acetate aqueous solution, while there was almost no difference in UZM-22 (see Table S2). Therefore, due to their lower Si/Al ratios (3.5 and 3.2 vs 5.0 and 4.8) the larger number of protons in H-ECR-1 and H-omega than in H-mordenite and H-UZM-22 can be exchanged with Cu^{2+} ions but, at the same time, they may induce a larger decrease in pH, and thus, induce a lower level of Cu^{2+}-exchange.

To prepare higher loadings of copper in H-mordenite and Na-omega, ion-exchange with a 0.01 M Cu^{2+} acetate aqueous solution was conducted up to five times. However, the copper loading of H-mordenite was still lower (4.1 vs 4.4 wt. %) than that of CuNa-mordeniteH and the latter was stagnant, even though its Cu/Al ratio (0.3) is still lower than 0.5. Copper-containing mordenite was also prepared by incipient wetness impregnation to yield 10 wt. % of copper. The powder XRD pattern (not shown) included the reflections of copper nitrate hydroxide. For the other large-pore zeolite samples listed in Table 1, the copper content was controlled by the concentration of the Cu^{2+} acetate aqueous solution (0.005 vs 0.01 M) and the ion-exchange cycles (1 to 3) from their Na-forms. For the other large-, medium-, and small-pore zeolites listed in the Supporting Information Table S1, only one type of copper-containing sample was prepared by stirring three times in 0.01 M Cu^{2+} aqueous solutions from their Na-forms.

Cu^{2+} ion-exchange in the zeolite pores caused a systematic decrease in the BET surface area of all the materials compared to their parent forms (see Tables 1, 2, and S1). In particular, the surface areas of CuNa-ECR-1H and CuNa-clinoptiloliteH decreased drastically to about 40 and 10 $m^2\ g^{-1}$, respectively, even though the amount of copper in CuNa-clinoptililiteH is rather low. The powder XRD patterns (not shown) of CuNa-ECR-1H and CuNa-clinoptiloliteH after nitrogen sorption showed that their structure was still intact. Thus, low values are due to copper in the zeolite micropores; the degree of the blockage

Table 2. Chemical composition and nitrogen sorption data for the Cu-zeolites prepared in this study.

Material[a]	IZA code	Si/Al	Cu (wt. %)	Cu/Al	BET surface area[d] ($m^2\ g^{-1}$)
CuNa-mordeniteH	MOR	8.5	4.1	0.38	390
CuNa-mordeniteH	MOR	5.0	4.4	0.30	-
CuH-mordeniteH			3.1	0.21	390
CuH-mordeniteH[b]			4.1	0.28	-
CuNa-mordeniteH[c]	MOR	6.0	10.0	0.69	-
CuNa-ECR-1H	EON	3.5	6.9	0.33	40 (250)[e]
CuNa-ECR-1L			2.9	0.14	370 (370)[e]
CuH-ECR-1H			2.0	0.09	-
CuNa-omegaH	MAZ	3.2	5.9	0.29	160
CuNa-omegaH[b]			6.0	0.29	-
CuNa-omegaL			2.4	0.12	-
CuH-omegaH			1.5	0.07	-
CuNa-PST-11H	MEI	3.4	8.4	0.47	540
CuNa-PST-11L			3.0	0.17	-
CuNa-UZM-22H	MEI	4.8	4.3	0.32	590
CuNa-UZM-22L			2.1	0.16	-
CuH-UZM-22H			4.2	0.31	-
CuNa-UZM-4H	BPH	3.0	9.2	0.61	470
CuNa-UZM-4L			3.1	0.20	-
CuNa-YH	FAU	3.0	7.6	0.32	750
CuNa-LH	LTL	2.7	4.2	0.20	350
CuNa-ZSM-5H	MFI	14.0	4.0	0.65	350
CuNa-clinoptiloliteH	HEU	5.8	2.5	0.18	10
CuNa-ferrieriteH	FER	8.9	3.6	0.38	250
CuNa-SUZ-4H	SZR	8.2	4.3	0.43	390
CuNa-SSZ-13H	CHA	15.8	4.5	0.84	640

[a] Prepared by stirring three times in 0.01 M (H) or one time in 0.005 M (L) Cu^{2+} aqueous solutions at room temperature for 24 h, unless stated otherwise. [b] Prepared by stirring five times in 0.01 M Cu^{2+} aqueous solutions. [c] Prepared by incipient wetness impregnation with $Cu(NO_3)_2$ solution. [d] Hyphen indicates no data. [e] The values in parentheses are of the samples after reaction activated at 450 °C.

Table 3. Methane-to-methanol conversion[a] over Cu-zeolites in this study.

Material[b]	IZA code	Channel system	Cu/Al	Extracted methanol[f] (μmol g-cat.$^{-1}$ / mmol mol-Cu^{-1})			
				Activation temperature (°C)			
				200	350	450	550
CuNa-mordeniteH	MOR	12- & 8-ring[e]	0.38	-	15.9 / 24.7	25.8 / 40.0	37.5 / 58.1
CuNa-mordeniteH	MOR	12- & 8-ring[e]	0.30	< 1 / < 1	12.4 / 18.0	21.0 / 30.4	32.2 / 46.5
CuH-mordeniteH	MOR	12- & 8-ring[e]	0.21	4.3 / 8.8	20.3 / 41.5	29.8 / 61.2	40.0 / 81.9
CuH-mordeniteH[c]	MOR	12- & 8-ring[e]	0.28	-	-	31.2 / 48.3	-
CuNa-mordeniteH[d]	MOR	12- & 8-ring[e]	0.69	-	-	< 1 / < 1	-
CuNa-ECR-1H	EON	12- & 8-ring[e]	0.33	-	18.3 / 16.8	19.7 / 18.1	7.1 / 6.5
CuNa-ECR-1L	EON	12- & 8-ring[e]	0.14	-	7.4 / 16.3	9.0 / 19.7	-
CuH-ECR-1H	EON	12- & 8-ring[e]	0.09	-	-	2.6 / 8.2	-
CuNa-omegaH	MAZ	12- & 8-ring[e]	0.29	3.9 / 4.1	53.3 / 57.4	86.1 / 92.8	72.0 / 77.6
CuNa-omegaL	MAZ	12- & 8-ring[e]	0.12	-	11.2 / 29.1	17.7 / 46.3	-
CuH-omegaH	MAZ	12- & 8-ring[e]	0.07	-	-	1.9 / 8.2	-
CuNa-PST-11H	MEI	12- & 8-ring[e]	0.47	-	13.8 / 10.5	21.5 / 16.3	15.2 / 11.5
CuNa-PST-11L	MEI	12- & 8-ring[e]	0.17	-	2.1 / 4.4	8.0 / 16.9	-
CuNa-UZM-22H	MEI	12- & 8-ring[e]	0.32	-	7.3 / 10.8	11.4 / 16.8	16.1 / 23.8
CuNa-UZM-22L	MEI	12- & 8-ring[e]	0.16	-	0.2 / 0.7	3.3 / 9.8	-
CuH-UZM-22H	MEI	12- & 8-ring[e]	0.31	-	-	13.6 / 20.6	-
CuNa-UZM-4H	BPH	12- & 8-ring[e]	0.61	-	2.8 / 1.9	8.0 / 5.5	5.9 / 4.1
CuNa-UZM-4L	BPH	12- & 8-ring[e]	0.20	-	0.2 / 0.5	2.1 / 4.3	-
CuNa-YH	FAU	12-ring	0.32	-	-	< 1 / < 1	-
CuNa-LH	LTL	12-ring	0.20	-	-	2.5 / 2.6	-
CuNa-ZSM-5H	MFI	10-ring	0.65	-	-	9.0 / 14.3	-
CuNa-clinoptiloliteH	HEU	8-ring	0.18	-	-	6.7 / 17.1	-
CuNa-ferrieriteH	FER	10- & 8-ring	0.38	-	-	10.4 / 18.3	-
CuNa-SUZ-4H	SZR	10-ring	0.43	-	-	14.4 / 11.5	-
CuNa-SSZ-13H	CHA	8-ring	0.84	-	-	30.0 / 42.4	-

[a] Activation: in a flow of pure oxygen (30 mL min^{-1}) at different temperatures (1 °C min^{-1}) for 4 h; Purge: in a flow of pure helium (30 mL min^{-1}) at 200 °C for 40 min; Reaction: in a flow of pure methane (15 mL min^{-1}) at 200 °C for 30 min; Methanol extraction: stirring with 2 mL deionized water for ca. 3 h. [b] Prepared by stirring three times in 0.01 M (H) or once in 0.005 M (L) Cu^{2+} aqueous solution at room temperature for 24 h, unless otherwise stated. [c] Prepared by stirring five times in 0.01 M Cu^{2+} aqueous solutions. [d] Prepared by incipient wetness impregnation with $Cu(NO_3)_2$ solution. [e] MEI structure is composed with 12- and 7-rings. [f] Hyphen indicates no data. The data related to omega materials are based on the omega mass in each sample.

may depend on the topology and chemical composition of the zeolite framework.[10,26] The BET surface area of CuNa-ECR-1H after reaction with methane activated at 450 °C increased again to 250 m^2 g^{-1}, which implies that the pore-blocking species changed to form active copper-oxo sites during the activation with oxygen and/or the reaction steps. It has been established that a redistribution of copper oxide occurs in zeolites.[27]

Catalyst activity

Table 3 shows the extracted methanol in μmol per weight of the reacted Cu-zeolites and mmol per mole of the copper-atom loaded on the zeolites after reaction with pure methane at different activation temperatures. Figures 3 – 5 present the selected data from Table 3 to more clearly discuss (see below). The amount of methanol produced by CuNa-mordeniteH with Cu/Al = 0.38 activated at 450 °C (26 μmol g-cat.$^{-1}$) is almost twice that obtained for the reported Cu-mordenite with a similar Cu/Al ratio (13 μmol g-cat.$^{-1}$, same activation temperature, but only 5% purity of methane).[6,12] Due to the higher amounts of extracted methanol, we tested all the samples using pure methane gas.

At first, to demonstrate the effect of the copper content on the conversion of methane-to-methanol, samples with different copper loadings were prepared for each large-pore zeolite as listed in Table 2. As expected, the amount of methanol produced increased with increasing copper content of each zeolite with the exception of Cu-mordenite and Cu-UZM-22 with a Si/Al ratio of about 5. The samples prepared from their H-forms had higher

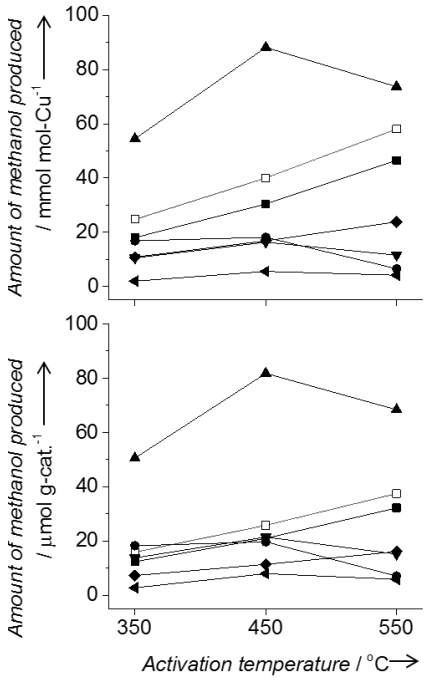

Figure 3. Methanol yields in µmol g-cat.$^{-1}$ (bottom) and mmol mol-Cu^{-1} (top) as a function of activation temperature under oxygen in methane-to-methanol conversion over CuNa-mordeniteH (□, Cu/Al = 0.38; ■, Cu/Al = 0.30), CuNa-ECR-1H (●), CuNa-omegaH (▲), CuNa-PST-11H (▼), CuNa-UZM-22H (◆), and CuNa-UZM-4H (◀).

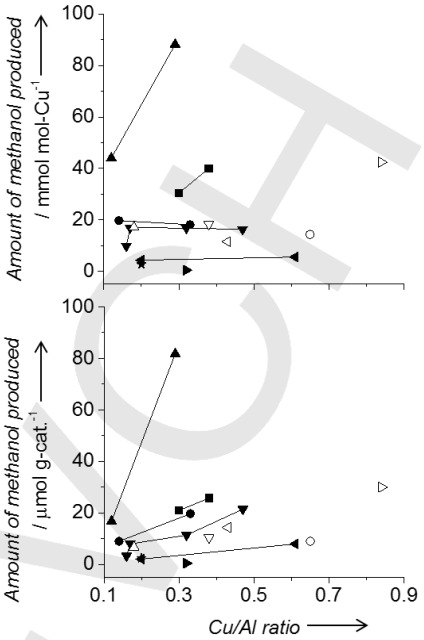

Figure 4. Methanol yields in µmol g-cat.$^{-1}$ (bottom) and mmol mol-Cu^{-1} (top) as a function of Cu/Al ratio of methane-to-methanol conversion, activated at 450 °C in a flow of oxygen over Cu-containing zeolite frameworks with different topologies prepared from their Na-forms: mordenite (■), ECR-1 (●), omega (▲), PST-11 and UZM-22 (▼), UZM-4 (◀), Y (▶), L (★), ZSM-5 (○), clinoptilolite (△), ferrierite (▽), SUZ-4 (◁), and SSZ-13 (▷).

methanol yields than those prepared from their Na-forms, despite the lower copper-loadings as discussed below. High copper-loadings may lead to an increase in the formation of active copper-oxo species inside the zeolite pores during the activation step, irrespective of the zeolite structure. The intrinsically higher aluminum content of PST-11 leads to higher copper-loading under identical ion-exchange conditions, as well as to a higher µmol methanol per weight of catalyst compared to that of UZM-22, even though both zeolites have the same framework topology (MEI). This illustrates the importance of zeolite synthesis to achieve novel framework compositions.[24] On the other hand, the CuNa-mordeniteH with 10 wt. % of copper content (Cu/Al = 0.69), prepared by impregnation, yielded almost no methanol (< 1 µmol g-cat.$^{-1}$), even though its copper content was more than twice as high as the other Cu-mordenite samples which may be due to copper species that were not well dispersed (e.g., large copper nitrate hydroxide particles), as described above. The methanol extraction procedure was repeated several times in our study, however there is still the possibility that the formed methoxy species were not extracted efficiently by the liquid extraction method, especially from the samples with high copper loadings.[10,26] CuNa-UZM-4H also contains large copper particles, as detected by powder XRD (see Figure S2) and also showed low methanol yields despite the fact that it has the highest copper content (9.2 wt. %, Cu/Al = 0.61) of the Cu^{2+} ion-exchanged samples in this study. Thus, well-dispersed copper is essential to produce methanol and the higher the wt. % of the copper is the higher the yield of methanol. In general, a low wt. % of copper yields less methanol, indicative of active sites with multiple copper ions.[3a,28]

Activation in oxygen at different temperatures influenced the formation of active copper-oxo species, as well as the related conversion of methane-to-methanol.[7,20] For Cu-ZSM-5, for example, there was an optimal activation temperature region (450 – 650 °C), and the methanol yield drastically decreased at higher than 700 °C.[7] Therefore, we tested the reaction at different activation temperatures over the copper-containing large-pore zeolites with differing amounts of copper prepared in this study (Table 3). Figure 3 shows the amount of methanol produced from the representative samples after activation at 350 450, and 550 °C in oxygen and consecutive interaction with methane at 200 °C, indicating that even higher yields can be obtained. In most cases, the amount of extracted methanol increased with increasing activation temperature. However, CuNa-ECR-1H, CuNa-omegaH, CuNa-PST-11H, and CuNa-UZM-4H yielded less methanol at 550 °C than the samples activated at lower temperature. These samples have high contents of copper (> 6 wt. %) due to their low Si/Al ratio (~3) (Table 2). Although their powder XRD patterns and TEM images after reaction at 550 °C activation temperature (see Figure S3 and Figure 2) revealed no large cuprous or cupric particles, the large amount of copper species may induce clustering at high activation temperature, leading to a loss of active copper-oxo sites. Therefore, it can be concluded that active copper-oxo species form at moderately higher activation temperature as

previously reported results,[7,20] especially in the zeolites containing the largest amount of copper.

The methanol yield obtained over CuNa-omegaH stands out. Compared with the second highest methanol yield of CuH-mordeniteH at 450 °C activation temperature, the methanol produced from CuNa-omegaH (86 vs 31 μmol g-cat.$^{-1}$ and 93 vs 61 mmol mol-Cu^{-1}) was almost three and 1.5 times higher in each μmol g-cat.$^{-1}$ and mmol mol-Cu^{-1}. This is the highest value of the catalysts in this study. The minor sodalite impurity in the sample (Figure 1) should yield a very low amount if any methanol because the Cu^{2+} ion-exchanged mixture of sodalite and omega, in which the proportion of sodalite is about 80% (see Figure S4), yielded only about 2 μmol g-cat.$^{-1}$. If there were no sodalite impurities, the produced methanol per weight of CuNa-omegaH at 450 °C activation temperature would probably be higher than 86 μmol g-cat.$^{-1}$.

Figure 4 compares the amount of methanol extracted from the CuNa-zeolites with a total twelve framework topologies after activation at 450 °C and as a function of Cu/Al ratio. At a similar Cu/Al ratio (~0.3), the methanol yields are ranged from 0 to 30 μmol g-cat.$^{-1}$ and from 0 to 40 mmol mol-Cu^{-1}, except for CuNa-omegaH which yields are ranged methanol up to 80 μmol g-cat.$^{-1}$ and 90 mmol mol-Cu^{-1}. The CuNa-omegaL with the lowest Cu/Al ratio (0.12) yields even greater amount of methanol (46 mmol mol-Cu^{-1}) than the CuNa-SSZ-13H with the highest Cu/Al ratio (0.84) does (42 mmol mol-Cu^{-1}). As shown in the Supporting Information Figure S5, the UV-Vis spectra of CuNa-zeolites, after activation in oxygen at 450 °C and subsequent reaction with methane at 200 °C, show diverse transition bands in the region between 15,000 and 30,000 cm^{-1} which indicate copper complexes containing bonds with extraframework oxygen. In particular, the spectrum of CuNa-ZSM-5H, activated under the same conditions, clearly shows the band centered at around 22,700 cm^{-1}, which was assigned to the mono-μ-oxo dicopper active species.[6] These results clearly show that there is probably significant structural diversity among the active copper-oxo species and, thus, the conversion of methane-to-methanol in this reaction system depends strongly on the topology of the zeolite framework. It is impossible to prepare all the Cu-zeolites with an identical Si/Al ratio and the same extent of aluminum pairing and, therefore, to control the Cu/Al ratio and copper speciation, making it more difficult to make a quantitative comparison among the different materials. Nonetheless, there are some trends and some electronic and steric factors of copper cations within the zeolite micropores that facilitate the formation of active sites, i.e., stabilization of di-, tri-, or even larger copper clusters, depending on the topology of the zeolite framework.[11,17,29]

The framework topology of zeolite omega, i.e., the MAZ structure, consists of 1D 12-MB ring channels and 3D 8-MB ring channels forming *gme*-cages, which are separated from each other (Table 1). To demonstrate the effect of 12-MB ring channels on the methane-to-methanol performance, we tested the copper-containing zeolites Y and L, both of which have only 12-MB ring pores with 3D and 1D connections, respectively (see Table S1). As shown in Figure 4, their methanol yields are the lowest (< 3 μmol g-cat.$^{-1}$) of the CuNa-zeolites in this study

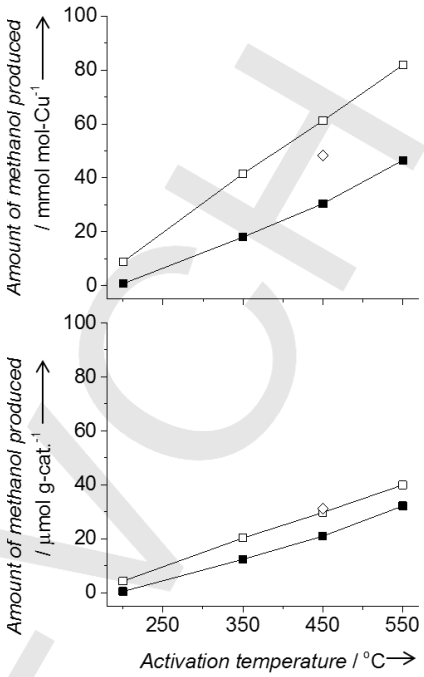

Figure 5. Methanol yields in μmol g-cat.$^{-1}$ (left) and mmol mol-Cu^{-1} (right) as a function of activation temperature under oxygen in methane-to-methanol conversion over CuNa-mordeniteH (■, Cu/Al = 0.30) and CuH-mordeniteH (□, Cu/Al = 0.21; ◇, Cu/Al = 0.28).

despite their copper-loadings being higher than 4 wt. %. The other copper-containing large- and medium-pore zeolites, composed of interconnected 12- and 8-MB ring channels and 10- and/or 8-MB ring channels, respectively, yielded different amounts of methanol. On the other hand, the amount of methanol extracted from CuNa-SSZ-13H, which is a unique zeolite with only 8-MB ring pores, was the second highest methanol yield (30 μmol g-cat.$^{-1}$ and 42 mmol mol-Cu^{-1}). The Cu/Al ratio of CuNa-SSZ-13H is the highest among the CuNa-zeolites due to the relatively low content of framework aluminum, i.e., the higher Si/Al ratio. Compared to CuNa-ZSM-5H with the Si/Al ratio of 14, which is similar to that of CuNa-SSZ-13H (16), the methanol yield is almost three times higher. This agrees with previous observations that small-pore zeolites had a high methanol yield, comparable to that of Cu-SSZ-13.[16-18]

The distribution of extraframework Na^+ ions of Na-omega zeolite has been reported from the crystallographic analysis.[22a] Those are non-randomly distributed and about 70% of Na^+ ions (ca. 6.9 among 9 Na^+ ions per unit cell) are located in the 3D 8-MB ring channels. If the Cu^{2+} ions in the zeolite omega in this study are also exchanged inside the 8-MB ring channels (about 70%, the same as the parent Na^+ ions), the copper content (4.1 vs 4.5 wt. %) is comparable to that of CuNa-SSZ-13H. The relatively high concentration of framework aluminum atoms (about 65%) in the 8-MB ring side pockets of mordenite represents the steric constraint to stabilize active copper-oxo species for the conversion of methane-to-methanol.[5] Therefore, it can be concluded that a high concentration of active copper-oxo sites may be achieved inside the independent 3D 8-MB ring

channels of zeolite omega which results in its high methane-to-methanol activity. If we consider the size of the molecules involved, the small-sized gases should experience the confinrment effect and interact to a greater extent with the Cu^{2+} ions, that are exchanged inside the small-pore channels to form the active copper-oxo species as well as to produce the methoxy species and finally to extract the methanol. Recently, some computational theoretical studies have reported that different metal-oxo active site geometries due to changes in zeolite ring-structures lead to changes in reactivity related to the amount of methanol yield.[17] The calculated activation energies for methane C-H bond dissociation by small-pore zeolites are lower than those for medium-pore zeolites.[17d] On the other hand, CuNa-SSZ-13H gave a considerably lower methanol yield despite the comparable copper content of each 8-MB ring pore structure. This implies that the large cage-like structure (i.e., cylindrical 20-hedral [$4^{12}6^{2}8^{6}$] *cha*-cage 6.7 Å in diameter and 10.0 Å in height in CHA framework topology) and the aluminum distribution may not be as favorable for the formation of active copper-oxo species. This speculation is supported by the result of CuNa-YH activated at 450 °C, which resulted in almost no methanol formed from the Cu^{2+} ion-exchanged materials. FAU-type, Y zeolite is very well-known as comprising both the biggest pore and *super*-cage (see Table S1).

The methanol yields of Cu-mordenite and Cu-UZM-22, prepared from their H-forms, are higher than those of their CuNa-forms, despite the same Si/Al ratios but lower copper-loadings, i.e., lower Cu/Al ratios (Table 3). Figure 5 shows that, at all different activation temperatures, CuH-mordeniteH with Cu/Al = 0.21 always gave higher methanol yields than those of CuNa-mordeniteH with Cu/Al = 0.30. Even under isothermal conditions with activation and reaction at 200 °C, CuH-mordeniteH still produced methanol. Furthermore, it was somewhat higher than the yield of methanol with CuNa-omegaH under the same reaction conditions (Table 3). This precursor effect is much stronger than the effect of copper content. As shown in Figure 5, at 450 °C activation in oxygen, CuH-mordeniteH with Cu/Al = 0.28 which is about 30% larger copper content than that of Cu/Al = 0.21 produced only a slightly larger amount of methanol μmol g-cat.$^{-1}$ and a lower methanol mmol mol-Cu^{-1}. There was no UV-Vis band at around 22,000 cm^{-1} in CuH-mordeniteH activated in oxygen at 450 °C (see Figure S5), even though the mono-μ-oxo dicopper site was revealed at around 22,000 cm^{-1} in CuNa-mordenite.[12] Narsimhan et al. reported that, upon the conversion of methane to acetic acid over Cu-mordenite by coupling oxidation with carbonylation reactions, the Cu-mordenite with Brønsted acid sites was drastically more active for carbonylation, due to the presence of a different active site for methane oxidation.[30] In this reaction, the co-produced methanol also increased with the increasing number of Brønsted acid sites. Thus, another new active site may also exist in our methane-to-methanol reaction system. The similar result has been also reported that among the Cu-mordenite zeolites prepared from diverse precusor cation types, CuH-mordenite showed the best methane-to-methanol activity.[19] We also tested CuH-ECR-1H and CuH-omegaH both of which have a Cu/Al ratio of < 0.1, but their methanol yields were much lower than those of their CuNa-forms, which may be due to the very low copper-loadings to produce the active copper-oxo species.

Conclusions

The characterization and catalytic results of many copper-loaded Na- and/or H-forms of large-pore zeolites (mordenite, ECR-1, omega, PST-11, UZM-22, and UZM-4) as well as other copper-containing large-, medium-, and small-pore zeolites (Y, L, ZSM-5, clinoptilolite, ferrierite, SUZ-4, and SSZ-13) for the stepwise oxidative conversion of methane-to-methanol indicate that the remarkable methanol yield of Cu^{2+} ion-exchanged zeolite omega is due to the highly dispersed copper-oxo active species inside the 3D 8-MB ring channels. Based on the results of our study, we propose four reliable rules for designing zeolite materials with regard to structure and chemistry for methane-to-methanol conversion. First, loading highly dispersed Cu^{2+} ions in the zeolite pores is essential. This depends on the parent Si/Al ratio as well as on the preparation method. Second, a higher activation temperature leads to the formation of more copper-oxo species, whereas too much copper yields less methanol. Third, the zeolite structure is one of the most important factors. The zeolite should preferably have 8-MB ring pore structure, rather than 10- or 12-MB ring systems, related to the confinement effect between the small methane gases and the active copper-oxo species formed inside the small-pore structure Finally, the Cu^{2+} ion-exchanged material prepared from the proton precursor helps to produce more methanol, even though the Cu^{2+} ion-exchange level is influenced by the parent Si/Al ratio.

Experimental Section

Catalyst preparation

The as-made forms of ECR-1, omega, PST-11, UZM-22, UZM-4, L, clinoptilolite, SUZ-4, and SSZ-13 were synthesized according to the procedures described in the literature.[22-24,31-33] Two Na-mordenite zeolites with Si/Al ratios of 8.5 and 6.0 and a Na-Y with a Si/Al ratio of 3.0 were obtained from ZeoChem. H-mordenite, NH_4-ZSM-5, and NaK-ferrierite zeolites with Si/Al ratios of 5.0, 14.0, and 8.9, respectively, were purchased from Tosoh. All the materials that were prepared using organic SDAs (i.e., TMA^+ and/or TEA^+ for omega, PST-11, and SUZ-4, choline for UZM-22, UZM-4, and L, and benzyltrimethylammonium for SSZ-13) were calcined in air at 550 °C for 10 h to remove the occluded organic species, with the exception of PST-11, which showed a serious structural collapse.[24] PST-11 was exchanged twice with 1.0 M $NaNO_3$ solutions (1.0 g solid per 100 mL solution) at 80 °C for 8 h, leading to a decrease of about 70 wt. % in the organic content, followed by calcination at 550 °C for 2 h. The as-prepared or calcined materials were converted to their Na-forms according to the same procedure given above. If required, before Cu^{2+} ion-exchange, some proton forms of the samples were prepared by refluxing twice in 1.0 M NH_4NO_3 solutions (1.0 g solid per 100 mL solution) for 8 h followed by calcination at 550 °C for 2 h. The large and small amounts of copper-loaded zeolites were prepared from the Na- and/or H-forms of precursor according to two different

procedures. The high-copper loaded samples were prepared by stirring three to five times in 0.01 M Cu^{2+} acetate aqueous solutions (1.0 g solid per 100 mL solution) at room temperature for 24 h; the low-copper loaded samples were prepared by stirring once in 0.005 M Cu^{2+} acetate solution. After the last exchange cycle, the samples were washed with a large amount of deionized water (> 1 L) to eliminate as many of the non-exchanged copper species in the zeolite pores as possible. Incipient wetness impregnation with $Cu(NO_3)_2$ solution was used to more increase the copper content. All the copper-loaded samples were dried at 110 °C for 10 h before the reaction. To determine the copper content, the samples underwent elemental analysis. To distinguish among the samples with different precursor types and copper loadings, CuNa- or CuH- and H or L are noted before and after the general zeolite material name, respectively. Prior to use as catalysts, the copper-loaded samples were granulated by placing them under a weight of maximum 5 tons, crushed, and sieved to obtain particles with a diameter of 250 to 500 µm.

Analytical methods

The crystallinity and the phase purity of the zeolites were determined by powder X-ray diffraction (XRD) by a PANalytical X'Pert diffractometer (Cu K_α radiation) with an X'Celerator detector. The powder XRD patterns of all as-prepared materials show that each is highly crystalline; there are no detectable impurity phases with the exception of zeolite omega, which contained a trace amount of sodalite (SOD) below 5% (see Figure S1). Elemental analysis was carried out by means of a Varian SpectrAA 220FS atomic absorption spectrophotometer. The nitrogen sorption experiments were performed in a Micromeritics Tristar II 3020 analyzer. All the copper-loaded samples were calcined in air at 550 °C for 2 h to remove the precursor salts before the elemental and N_2 sorption measurements. The relatively lower BET surface area (360 m^2 g^{-1}) of calcined zeolite omega (Table 1) probably originates from the relatively larger crystal size (1 - 5 µm) compared to the other zeolites (see Figure S6). Crystal morphology and average particle size were determined by a Tecnai F30 ST transmission electron microscope (TEM), operating at an acceleration voltage of 300 kV. The diffuse reflectance UV-Vis spectra of Cu^{2+} ion-exchanged samples were recorded on an Agilent Cary 4000 spectrometer at scan rate of 9,000 cm^{-1} min^{-1} from 12,500 to 35,000 cm^{-1} after activation in an oxygen flow at 450 °C for 3 h and subsequently after reaction with methane at 200 °C for 1 h.

Reacting methane

The reaction of methane-to-methanol was conducted under atmospheric pressure in a continuous-flow fixed-bed microreactor containing about 0.5 g of a copper-loaded zeolite sieve fraction.[12-14] Each catalyst was activated in a flow of pure oxygen (30 mL min^{-1}) by heating to desired temperature (200, 350, 450, or 550 °C) at a ramping rate of 1 °C min^{-1}, kept at the desired temperature for 4 h, and then cooled to 200 °C (1 °C min^{-1}). After activation, the catalyst bed was flushed by streams of a pure helium (30 mL min^{-1}) for 40 min at the given temperature. Then, pure methane (15 mL min^{-1}) was fed into the microreactor at the same temperature. After interaction with methane at 200 °C for 30 min, the methane flow was stopped, and the catalyst bed was cooled to room temperature in a flow of helium (30 mL min^{-1}). For methanol extraction, the reacted catalyst was stirred with 2 mL deionized water at room temperature. After stirring for about 3 h, a clear solution was collected by filtering the mixture and made up to 2 mL by adding deionized water and 10 µL acetonitrile (10 vol % in aqueous solution) as an internal standard. The resulting solution was analyzed by an Agilent 6890 gas chromatograph equipped with a Restek Rtx®-5 column (3 m x 0.25 mm) and a flame ionization detector. The liquid extraction procedure was repeated more than two times, and the final methanol yield was determined by adding the all extractions. The amount of methanol extracted after the second extraction was always 10% lower than the first.

Acknowledgements

We are grateful for the financial support of the postdoctoral fellowship provided by the Swiss government excellence scholarship by the federal commission for scholarships for foreign students (FCS). We thank Mr. Ali Mansouri for the UV-Vis measurements, Dr. Frank Krumeich for the TEM measurements, and Dr. Selmi E. Bozbag for the help with the experiments.

Keywords: copper • heterogeneous catalysis • methane • methanol • zeolites

[1] a) A. Holmen, *Catal. Today* **2009**, *142*, 2; b) C. Hannond, S. Conrad, I. Hermans, *ChemSusChem* **2012**, *5*, 1668; c) R. Horn, R. Schlögl, *Catal. Lett.* **2015**, *145*, 23.

[2] a) E. M. C. Alayon, M. Nachtegaal, M. Ranocchiari, J. A. van Bokhoven, *Chimia* **2012**, *66*, 668; b) R. A. Himes, K. Barnese, K. D. Karlin, *Angew. Chem.* **2010**, *122*, 6864; *Angew. Chem. Int. Ed.* **2010**, *49*, 6714.

[3] a) M. H. Groothaert, J. A. van Bokhoven, A. A. Battiston, B. M. Weckhuysen, R. A. Schoonheydt, *J. Am. Chem. Soc.* **2003**, *125*, 7629; b) J. S. Woertink, P. J. Smeets, M. H. Groothaert, M. A. Vance, B. F. Sels, R. A. Schoonheydt, E. I. Solomon, *Proc. Natl. Acad. Sci. U.S.A.* **2009**, *106*, 18908.

[4] a) S. Grundner, M. A. C. Markovits, G. Li, M. Tromp, E. A. Pidko, E. J. M. Hensen, A. Jentys, M. Sanchez-Sanchez, J. A. Lercher, *Nat. Commun.* **2015**, *6*, 7546; b) G. Li, P. Vassilev, M. Sanchez-Sanchez, J. A. Lercher, E. J. M. Hensen, *J. Catal.* **2016**, *338*, 305; c) D. Palagin A. J. Knorpp, A. B. Pinar, M. Ranocchiari, J. A. van Bokhoven, *Nanoscale* **2017**, *9*, 1144.

[5] V. I. Sobolev, K. A. Dubkov, O. V. Panna, G. I. Panov, *Catal. Today* **1995**, *24*, 251.

[6] M. H. Groothaert, P. J. Smeets, B. F. Sels, P. A. Jacobs, R. A. Schoonheydt, *J. Am. Chem. Soc.* **2005**, *127*, 1394.

[7] P. J. Smeets, M. H. Groothaert, R. A. Schoonheydt, *Catal. Today* **2005**, *110*, 303.

[8] P. J. Smeets, R. G. Hadt, J. S. Woertink, P. Vanelderen, R. A. Schoonheydt, B. F. Sels, E. I. Solomon, *J. Am. Chem. Soc.* **2010**, *132* 14736.

[9] P. Vanelderen, R. G. Hadt, P. J. Smeets, E. I. Solomon, R. A. Schoonheydt, B. F. Sels, *J. Catal.* **2011**, *284*, 157.

[10] N. V. Beznis, B. M. Weckhuysen, J. H. Bitter, *Catal. Lett.* **2010**, *138*, 14.

[11] C. Hammond, N. Dimitratos, R. L. Jenkins, J. A. Lopez-Sanchez, S. A. Kondrat, M. H. ab Rahim, M. M. Forde, A. Thetford, S. H. Taylor, H. Hagen, E. E. Stangland, J. H. Kang, J. M. Moulijn, D. J. Willock, G. J. Hutchings, *ACS Catal.* **2013**, *3*, 689.

[12] E. M. C. Alayon, M. Nachtegaal, M. Ranocchiari, J. A. van Bokhoven, *Chem. Commun.* **2012**, *48*, 404.

[13] E. M. C. Alayon, M. Nachtegaal, E. Kleymenov, J. A. van Bokhoven, *Microporous Mesoporous Mater.* **2013**, *166*, 131.

[14] E. M. C. Alayon, M. Nachtegaal, A. Bodi, J. A. van Bokhoven, *ACS Catal.* **2014**, *4*, 16.

[15] E. M. C. Alayon, M. Nachtegaal, A. Bodi, M. Ranocchiari, J. A. van Bokhoven, *Phys. Chem. Chem. Phys.* **2015**, *17*, 7681.

[16] M. J. Wulfers, S. Teketel, B. Ipek, R. F. Lobo, *Chem. Commun.* **2015**, *51*, 4447.
[17] a) A. R. Kulkarni, Z.-J. Zhao, S. Siahrostami, J. K. Nørskov, F. Studt, *ACS Catal.* **2016**, *6*, 6531; b) M. H. Mahyuddin, A. Staykov, Y. Shiota, K. Yoshizawa, *ACS Catal.* **2016**, *6*, 8321; c) F. Göltl, C. Michel, P. C. Andrikopoulos, A. M. Love, J. Hafner, I. Hermans, P. Sautet, *ACS Catal.* **2016**, *6*, 8404; d) M. H. Mahyuddin, A. Staykov, Y. Shiota, M. Miyanishi, K. Yoshizawa, *ACS Catal.* **2017**, *7*, 3741.
[18] K. Narsimhan, K. Iyoki, K. Dinh, Y. Román-Leshkov, *ACS Cent. Sci.* **2016**, *2*, 424.
[19] S. Grundner, W. Luo, M. Sanchez-Sanchez, J. A. Lercher, *Chem. Commun.* **2016**, *52*, 2553.
[20] P. Tomkins, A. Mansouri, S. E. Bozbag, F. Krumeich, M. B. Park, E. M. C. Alayon, M. Ranocchiari, J. A. van Bokhoven, *Angew. Chem.* **2016**, *128*, 5557; *Angew. Chem. Int. Ed.* **2016**, *55*, 5467.
[21] Ch. Baerlocher, L. B. McCusker, Database of Zeolite Structures: http://www.iza-structure.org/databases/.
[22] a) J. Shin, N. H. Ahn, S. J. Cho, L. Ren, F.-S. Xiao, S. B. Hong, *Chem. Commun.* **2014**, *50*, 1956; b) J. Song, L. Dai, Y. Ji, F.-S. Xiao, *Chem. Mater.* **2006**, *18*, 2775; c) R. Jarman, A. Jacobson, M. Melchior, *J. Phys. Chem.* **1984**, *88*, 5748.
[23] M. A. Miller, J. G. Moscoso, S. C. Koster, M. G. Gatter, G. J. Lewis, *Stud. Surf. Sci. Catal.* **2007**, *170*, 347.
[24] M. B. Park, S. H. Ahn, N. H. Ahn, S. B. Hong, *Chem. Commun.* **2015**, *51*, 3671.
[25] Y. Zhang, K. M. Leo, A. F. Sarofim, Z. Hu, M. Flytzani-Stephanopoulos, *Catal. Lett.* **1995**, *31*, 75.
[26] N. V. Beznis, A. N. C. van Laak, B. M. Weckhuysen, J. H. Bitter, *Microporous Mesoporous Mater.* **2011**, *138*, 176.
[27] P. N. R. Vennestrøm, T. V. W. Janssens, A. Kustov, M. Grill, A. Puig-Molina, L. F. Lundegaard, R. R. Tiruvalam, P. Concepción, A. Corma, *J. Catal.* **2014**, *309*, 477.
[28] M. H. Groothaert, K. Lievens, H. Leeman, B. M. Weckhuysen, R. A. Schoonheydt, *J. Catal.* **2003**, *220*, 500.
[29] T. Ymura, M. Takeuchi, H. Kobayashi, Y. Kuroda, *Inorg. Chem.* **2009**, *48*, 508.
[30] K. Narsimhan, V. K. Michaelis, G. Mathies, W. R. Gunther, R. G. Griffin, Y. Román-Leshkov, *J. Am. Chem. Soc.* **2015**, *137*, 1825.
[31] G. Seo, M.-W. Kim, J.-H. Kim, B. J. Ahn, S. B. Hong, Y. S. Uh, *Catal. Lett.* **1998**, *55*, 105.
[32] M. A. Asensi, M. A. Camblor, A. Martinez, *Microporous Mesoporous Mater.* **1999**, *28*, 427.
[33] M. Itakura, I. Goto, A. Takahashi, T. Fujitani, Y. Ide, M. Sadakane, T. Sano, *Microporous Mesoporous Mater.* **2011**, *144*, 91.

Entry for the Table of Contents (Please choose one layout)

Layout 1:

FULL PAPER

We propose four reliable design rules for copper zeolites for conversion of methane-to methanol: i) composed with small-pores; ii) containing large amount of copper content in a well-dispersed manner; iii) activated at moderately high temperature under flowing oxygen; iv) prepared from proton form precursor.

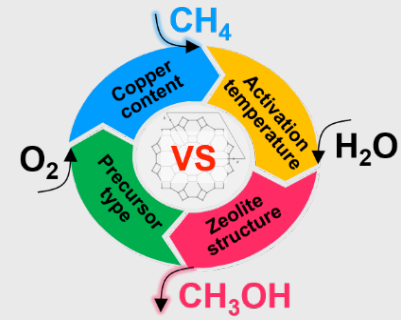

*Min Bum Park, Sang Hyun Ahn, Marco Ranocchiari, Jeroen A. van Bokhoven**

Page No. – Page No.

Comparative Study of Diverse Cu-Zeolites for Conversion of Methane-to-Methanol